Mechanisms of pit formation at strained crystalline Si(111)/Si_3N_4(0001) interfaces: Molecular-dynamics simulations

Martina E. Bachlechner,[1] Deepak Srivastava,[2] Eli T. Owens,[1] Jarrod Schiffbauer,[1] Jonas T. Anderson,[1,*] Melissa R. Burky,[1,3] Samuel C. Ducatman,[1,4,†] Adam M. Gripper,[1,‡] Eric J. Guffey,[1,4,5,§] and Fernando Serrano Ramos[1,6]

[1]*Physics Department, West Virginia University, Morgantown, West Virginia 26506, USA*

[2]*NASA Ames Research Center, MS T229-1, Moffett Field, California 94035, USA*

[3]*Chemistry Department, Davis & Elkins College, Elkins, West Virginia 26241, USA*

[4]*University High School, Morgantown, West Virginia 26505, USA*

[5]*NASA Independent Verification and Validation Facility Science and Engineering Apprenticeship Program*

[6]*Department of Computer Science, Metropolitan University, San Juan, Puerto Rico 00928*

(Received 12 June 2006; published 21 August 2006)

Molecular-dynamics simulations of the crystalline silicon-silicon nitride interfaces are performed to investigate the mechanical failure mechanisms at the interfaces under external strain. At 8% applied tensile strain, parallel to the interface, regular crack initiation and propagation in silicon nitride and dislocation emission and propagation in silicon are observed. At larger 16% strain, however, the formation of a pit similar to that in experiments with lattice-mismatched systems is observed. The simulation results suggest the primary mechanism of pit formation is interaction of a local compressional pinch of the film at the interface with the close proximity to the arrival of a dislocation at the interface in the highly strained silicon.

DOI: 10.1103/PhysRevB.74.075327 PACS number(s): 68.35.−p, 62.20.Mk, 31.15.Qg

I. INTRODUCTION

The understanding of structure, stability, and mechanisms of mechanical failure at crystalline interfaces in semiconductor thin films and quantum dots is increasingly important in the electronics and quantum devices fabrication technologies. As the feature and control sizes of such devices continue to shrink, the contribution of the interface strain induced defects, towards the inefficient operation or failure of such devices, also increases significantly. Therefore, pit formation and growth have been studied experimentally in great detail as these pits alter the electronic, optical, and magnetic properties of semiconducting and magnetic materials substantially.[1–12]

Silicon carbide (SiC), e.g., is a material of great interest for high-temperature, high-power, and high-frequency electronics. However, crystal defects, in particular pits at the interface of 3C-SiC/Si, significantly influence the quality of the overgrown 3C-SiC films,[1,2] Tungsten silicide (WSi_x) used as Schottky gate metallization in self-alligned GaAs metal semiconductor field effect transistor (MESFET) and heterostructure field effect transistor (HFET) devices is found to induce pit formation in GaAs for a certain range of WSi_x compositions.[3] SiGe alloy films grown on silicon have been shown to exhibit strain relaxation by pit formation.[4,5] Also nitride alloys (GaN, AlGaN, and InGaN) with applications in both electronic and optical devices exhibit pit formation for a certain range of $Al_xGa_{1-x}N$ (Refs. 8 and 9) and $In_xGa_{1-x}N$ (Ref. 10) compositions. Sharma *et al.*[11] investigated InGaN multiple quantum wells, which are of interest for applications as very bright LEDs and lasers, and found that lower temperatures of InGaN/GaN quantum-well growth assist the formation of pits. Co thin films as used in giant magnetoresistive (GMR) devices are found to have pit concentrations decreasing exponentially with the film thickness.[12]

A few proposed explanations of the pit formation at the interface in particular include: (a) the influence of thermal annealing during cleaning,[1,2,7] (b) the effect of surface chemistry at the interfaces during the growth of the films,[1,2] (c) the influence of lattice-mismatch strain[2] (and of strain reduction via buffer layers), and (d) out diffusion of substrate atoms.[2,3,11] None of these proposed mechanisms has been observed or validated directly.

Concurrently, on the other hand, atomistic computer simulations have become important in providing atomistic details and mechanisms of processes and structures that are not readily possible to investigate through experimental means.[13–15] Comprehensive simulations have been performed on the continuum,[16–18] the atomistic,[19–25] and the quantum-mechanical[26–28] scales to investigate mechanical and structural properties in various materials. In particular, kinetic Monte Carlo simulations have been used to simulate (i) etching that results in surface and edge pits,[29] (ii) pit evolution at prepitted surfaces,[30] and (iii) morphology evolution of strained epitaxial film resulting in pit formation.[31] However, the authors are not aware of any atomistic simulations of buried pits as they occur during the growth of silicon carbide on silicon[1,2] and WSi_x on GaAs.[3]

Using extensive molecular-dynamics (MD) simulations of Si/Si_3N_4 under externally applied tensile strain parallel to the interfaces, for the first time, we observe the formation of the pits at the interfaces. These simulation results will be important to determine the possible causes and ultimately control methodologies for such defects.

II. Si(111)/Si_3N_4(0001) INTERFACE MODEL AND METHOD

The Si(111)/Si_3N_4(0001) interface is taken to be atomically sharp,[32] justified experimentally by Kim and Yeom.[33] In our model of the Si(111)/Si_3N_4(0001) interface[32] we distin-

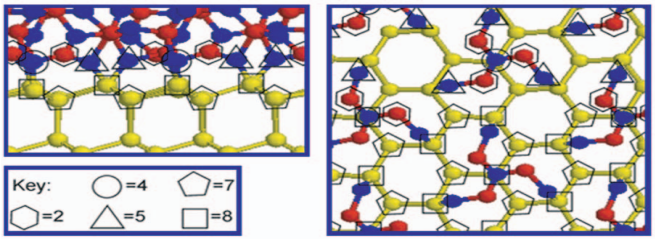

FIG. 1. (Color) Side (left) and top (right) views of the $Si(111)/Si_3N_4(0001)$ interface representing the eight different atom types. Yellow: silicon atoms in silicon; blue: nitrogen atoms in silicon nitride; red: silicon atoms in silicon nitride. Interface atoms are further distinguished using the polygon key.

guish between a total of eight different atom types to account for the different environments that silicon and nitrogen atoms experience in bulk and interface silicon and silicon nitride, respectively. Bulk silicon nitride consists of type 1 silicon and type 3 nitrogen atoms; the silicon nitride interface layer consists of type 2 silicon, and types 4 and 5 nitrogen atoms (see Fig. 1). The model accounts for the difference between the fully bonded type 4 nitrogen atoms and the initially twofold bonded type 5 nitrogen atoms in the interface plane. In the silicon, the type 6 silicon atoms are the bulk silicon atoms, the type 7 silicon atoms are fully bonded silicon atoms at the interface double layer, and the type 8 silicon atoms are threefold bonded silicon atoms at the interface double layer.

LCAO (linear combination of atomic orbitals) electronic structure calculations[34,35] for the crystalline $Si(111)/Si_3N_4(0001)$ interface have shown that the interface affects the electronic charges within a single layer of the layered $Si_3N_4(0001)$ film (the layer separation is about 1.3 Å) and the top-most double layer in Si(111). In our simulations we have not observed any mixing of atoms at the interface, i.e., no Si atoms from silicon move into silicon nitride and no Si or N atoms from silicon nitride move into the silicon system. Therefore, the atom types have been kept fixed throughout the simulations presented here. The analyses presented here, fully take advantage of having detailed information for the different atom types, in particular the atoms in the interface layers of silicon nitride and silicon, respectively.

In a molecular-dynamics simulation, the velocities and positions of all the atoms in a system are obtained by numerically integrating Newton's equations of motion using the velocity-Verlet algorithm and an appropriate potential energy function. Due to silicon's wide range of applications several interaction potentials between Si atoms within silicon systems have been developed (for a review see, e.g., Balamane *et al.*[36]) and used in a variety of simulations including Stillinger and Weber,[37] Tersoff,[38,39] Chelikowsky,[27] Cook and Clancy,[40] Juan *et al.*,[41] Bazant *et al.*,[42] Justo *et al.*,[28] Choudhary and Clancy,[43] Demkowicz and Argon,[44,45] and Posselt *et al.*[46] In a comparative study Nurminen *et al.*[47] find that for surface reconstruction and finite-temperature simulations the Stillinger/Weber potential[37] gives the best overall performance compared to Tersoff potentials[38,39] that are based on bond order. In the context of fracture, it should be noted that the Stillinger/Weber potential as well as environment-dependent potentials[28,42] do not yield brittle crack propagation as is seen in silicon experimentally at room temperature. Marder and collaborators[48–50] observe brittle fracture in silicon when modifying the original Stillinger/Weber potential by doubling the strength of the term enforcing fixed angles between bonds. As will be described below, the simulations presented here are at 600 K and therefore near the experimental brittle-to-ductile transition temperature where the Stillinger/Weber potential yields the correct mechanical response. The Stillinger/Weber potential has also been used to successfully describe fluorination of Si(100) surfaces[51–55] and the interaction of hydrogen with silicon surfaces.[56] These authors focus their discussion on the qualitative agreement of the different structural and dynamical features investigated. Interactions between Si atoms and F atoms, for example, have been through first-principles-derived Stillinger-Weber-type potentials. As described later, a first-principles-based approach has been adapted also for the silicon/silicon nitride interface potential.[32]

In the simulations presented here, the Si-Si atomic interactions in bulk are described by the Stillinger-Weber[37] potential for silicon. However, to separate the effect of initial lattice mismatch between silicon and silicon nitride, and to perfectly lattice-match the two systems, the original parameter $\sigma=0.209\,51$ nm in the Stillinger-Weber potential[37] was modified to $\sigma=0.213\,70$ nm. The silicon nitride potential[57] consists of two-body terms that account for Coulomb interactions, the steric repulsion, and the charge-dipole interactions, as well as, three-body terms describing the stretching and bending of the bonds. This potential has proven to provide excellent descriptions of mechanical and structural properties of crystalline, amorphous, and nanophase silicon nitride.[58–60]

Our model for the Si/Si_3N_4 interface[32] distinguishes between Si atoms in the silicon substrate and Si and N atoms in the silicon nitride film. Since the atoms at or near the interface have different charge transfer they have to be treated differently. Based on LCAO electronic structure calculations[34,35] for the crystalline $Si(111)/Si_3N_4(0001)$ interface, we find that this system may be adequately modeled as an eight-component system (see Fig. 1). Two-by-two unit cells of Si(111) correspond to one unit cell of $Si_3N_4(0001)$ in the respective interface planes. Si atoms in the top layer of silicon form bonds to N atoms in the bottom layer of silicon nitride leaving dangling bonds of Si atoms in the interface layer of silicon nitride. The interface interaction model assumes that the bond lengths and the bond angles at and across the interface are comparable to those in bulk silicon nitride.

In a film geometry, surface and interface atoms tend to heat up. The standard method of scaling velocities of all the atoms with a common scaling factor would not suffice in this situation. Therefore, the system temperature is maintained by using Langevin dynamics[61] in which atoms experience a damping depending on their respective velocities as well as an additional stochastic velocity. In order to achieve computational speed up, the multiple-time step method developed by Tuckerman *et al.*[62] is implemented. Depending on the stage of the simulation, a time step of 2 or 6 fs is used and long-range forces are calculated only every other time step.

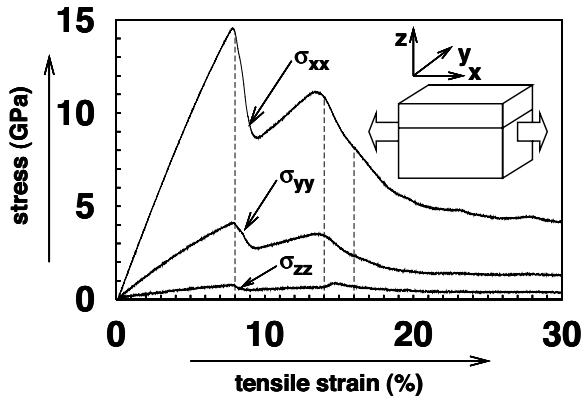

FIG. 2. Stress-versus-strain graphs for the diagonal stress tensor components σ_{xx}, σ_{yy}, and σ_{zz}, respectively. Inset: Atomic-scale view of the $Si(111)/Si_3N_4(0001)$ interface indicating direction of applied strain.

Since the investigation focuses on the mechanical properties of silicon with a silicon nitride film, a simulation system preparation scheme that does not describe the growth process has been employed. The free surfaces in both silicon nitride and silicon separated by 6 Å are first equilibrated at 0 K, and then brought together gradually by moving them in steps of 0.5 Å closer to each other followed by relaxation.[32] The system is heated to 300 K and equilibrated, after which the temperature is increased to 600 K followed by expansion and additional equilibration to obtain a minimum stress configuration.

III. RESULTS AND DISCUSSION

The MD system simulated consists of a total of 668 160 atoms. The lateral dimensions at 600 K are 270 Å and 280 Å. A 44-Å-thick Si_3N_4 film is placed on a 95-Å-thick Si substrate and the interface system is stretched by "holding" a slice of 8 Å on each end along the x direction. These atoms are then pulled (see inset in Fig. 2) at a constant strain rate of 2.5×10^9 s^{-1} using a time step of 2 fs. While the applied strain rate is orders of magnitude larger than what would ever be possible in experiments, it is possible to simulate the defect formation processes at such high strain rates to extract the physical mechanism and later develop models that are applicable at experimentally feasible strain rate, temperatures, and length scale.[19]

The tensile strain is applied parallel to the interface (see inset in Fig. 2), i.e., in the [2 1 0 0] direction for Si_3N_4 and the [−2 1 1] direction for Si, with periodic boundary conditions used in the y direction. Therefore, the system cannot shrink in the y direction and builds up stresses, σ_{yy}, following on average the features of σ_{xx} in the course of the simulation (see Fig. 2). The stresses σ_{xx}, σ_{yy}, and σ_{zz} build up linearly with the applied strain according to linear elasticity theory. The stresses increase elastically until a significant drop occurs at about 8% of the applied strain. This drop can be attributed to the stress release due to crack initiation and propagation in silicon nitride layers. A crack first opens on the left side of the film followed by another one on the right side of the film [Figs. 3(b)–3(d)].

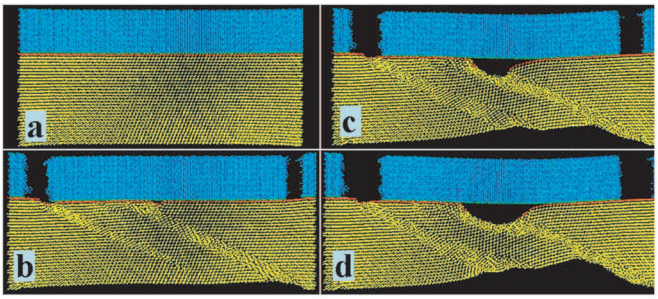

FIG. 3. (Color). Atomic positions in the Si/Si_3N_4 interface at (a) 7%, (b) 16%, (c) 23%, and (d) 30% of strain. Yellow: silicon, blue: Si_3N_4, red: interface layers.

An island of Si_3N_4 thus breaks off from the left and right side of the film, and, again on average, the bonds relax to the unstrained value for Si_3N_4. This is determined via analysis of pair distribution functions calculated from the appropriate atomic configurations.[63] While the bulk of the Si_3N_4 film is approximately strain free, local portions of the Si_3N_4 side of the interface are undergoing lateral compression (see Fig. 4), starting between 8–10 % when the cracks form. In particular, a persistent local compressional pinch appears in the region where the formation of the pit is later observed.

The stresses continue to increase in Si as the system is stretched until about 14% strain, where stress is relieved by dislocation emission in Si. Two dislocations are observed. One dislocation starts beneath the left crack in Si_3N_4 and subsequently moves from the interface towards the free surface where the slip creates a step. The other occurs at a parallel slip plane to the right at the free bottom silicon sur-

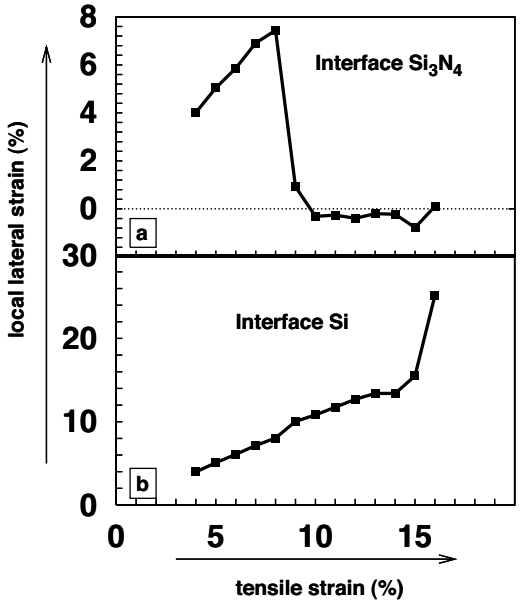

FIG. 4. Local interfacial lateral strains at the location of the pit as a function of externally applied strain. (a) Averaged over silicon nitride interface atoms, and (b) averaged over silicon interface atoms.

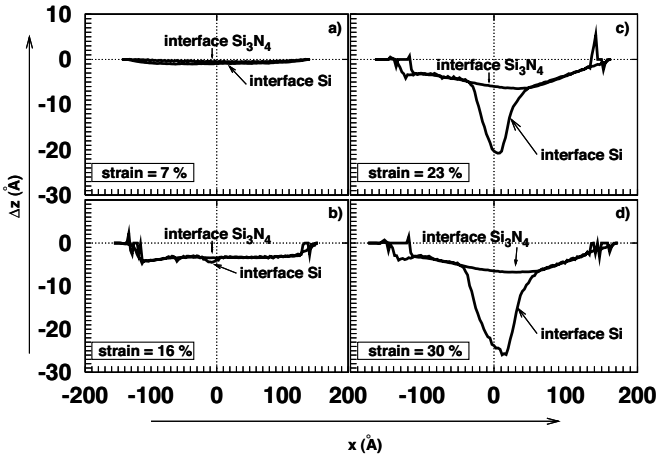

FIG. 5. Average displacement in z-direction in a slice in x direction, i.e., Δz versus the position of the slice at (a) 7%, (b) 16%, (c) 23%, and (d) 30% of strain. Interface Si_3N_4: averages over the atoms in the Si_3N_4 interface layer only, interface Si: averages over the atoms in the silicon interface double layer only.

face and propagates towards the interface [see Fig. 3(b)] arriving at 15% at the interface near the location of the compressional pinch that subsequently develops into the pit. Immediately prior to the appearance of the pit, the local lateral compressional strain in the interface Si_3N_4 layers is approximately 1.5%, compared to the local lateral tensile expansion of the interface Si layers which ranges from 10–15 % local strain between 9–16 % external strain. At 16% external strain, the pit forms and grows in the strained silicon phase to provide a mechanism of strain release or relaxation [see Fig. 3(b)] and is located just below the center of the Si_3N_4 island. The analyses presented here suggests that the nucleation of the pit corresponds to the interaction of the local lateral compression of the film, occurring at a value of applied strain lower than 16%, with the close proximity to the arrival of a dislocation at the interface in the highly strained silicon.

To further investigate the formation and growth of the pit the average z displacements of the interface atoms in Si_3N_4 and in Si double layers are analyzed separately and shown in Fig. 5. At 7% strain [Fig. 5(a)], both the Si_3N_4 and the Si interface layers show very small vertical displacements. Figure 5(b) shows the visible onset of the pit at 16% strain, where both Si and Si_3N_4 interface layer atoms show average negative z displacements. The relaxed Si_3N_4 interface layer atoms do not show much further increase in the negative z displacements, whereas the strained Si interface layer atoms show large increase in the negative z displacements indicating the growth of the pit in Figs. 5(c) and 5(d) at the larger tensile strains of 23% and 30% where it grows by downward movement of Si double layer atoms. Detailed analysis showed that (a) the pit grows asymmetrically more in the positive direction, and (b) that both pit width and depth increase rapidly after the onset at 16% strain. The pit depth positions also showed that Si_3N_4 interface layers stay at about the same z coordinate and the pit grows by movement of Si double layer atoms downward.

IV. SUMMARY AND CONCLUSION

In summary, from the above analyses of the vertical displacement of interfacial atoms it is clear that (a) the Si_3N_4 island is essentially strain free after breaking off due to crack initiation and propagation on both sides, (b) the tensile strain in Si layers parallel to the interface continue to build up while several small regions of local compressional strain or pinch form in the Si_3N_4 interface layer. Strain induces dislocation slip in the bulk Si, which in combination with the compressional pinch at the interface nucleates a pit, and (c) as tensile strain on the Si layers continue to increase, the interface atoms in Si layers move away from the interface causing the growth of the pit at the interface. The experimental observation that larger lattice-mismatch strain enhances the likelihood of pit formation[11] supports the above mechanism. The above suggests a general mechanism of pit formation for lattice-mismatched systems by which pits nucleate at a site of local compressional strain where the substrate film interface is possibly weakened by slip of the underlying substrate, and the visible pit forms. This process is not explicitly dependent upon surface or interface chemical effects as suggested recently in the experimental literature.[1,2,7] However, the possible effects of surface chemistry at the growing interface, e.g. augmentation of pit formation and growth, need to be investigated in future studies.

Additionally, as mentioned above, the pit formation and growth mechanism depend on the kinetic temperature of the simulations and the applied tensile strain rate. Preliminary results show the formation of similar pits at the same strain rate at 300 and 900 K simulations, as well as at 600 K and twice the strain rate of the present simulation. A systematic study to investigate the temperature and strain rate dependence of the kinetics of pit nucleation and growth is currently underway and will be published elsewhere.

Although the model of the interface used here could be improved by incorporating quantum modeling as charge transfers may change in the course of the simulation we are confident that our conclusions regarding the relationship between strain-relaxation and interfacial failure mechanisms are comparable to those in heteroepitaxial structures with high lattice mismatch as found in Si/SiC systems.[1,2]

In combination with the experimental observations, these atomistic computational studies lay the foundation for understanding and offer the possibility of control of pit formation at lattice-mismatched interfaces with significant technological implications.

ACKNOWLEDGMENTS

The authors acknowledge support from NASA WV Space Grant Consortium, NASA IV&V Facility (SEAP), and the WVU Summer Undergraduate Research Experience (SURE) Program funded by WV EPSCoR. J.T.A. and F.S.R. acknowledge support from the National Science Foundation CISE REU program Grant No.0353806. Part of this work (D.S.) is supported by NASA Contract No. NAS2-03144 to UARC.

*Present address: The University of New Mexico, Albuquerque, NM 87131
†Present address: Grinnell College, Grinnell, Iowa 50112
‡Present address: Naval Nuclear Power Training Command, 101 NNPTC Circle, Goose Creek, SC 29445
§Present address: Massachusetts Institute of Technology, 77 Massachusetts Avenue, Cambridge, MA 02139–4307

[1] K. C. Kim, C. I. Park, Jae I. Roh, K. S. Nahm, and Y. H. Seo, J. Vac. Sci. Technol. A **19**, 2636 (2001).
[2] K. S. Ziemer, "*Studies of the Initial Stage of Silicon Carbide Growth on Silicon*," Ph.D. thesis, West Virginia University, 2001.
[3] A. G. Lahav, C. S. Wu, and F. A. Baiocchi, J. Vac. Sci. Technol. B **6**, 1785 (1988).
[4] L. Di Gaspare, E. Palange, G. Capellini, and F. Evangelisti, J. Appl. Phys. **88**, 120 (2000).
[5] K. M. Chen, D. E. Jesson, S. J. Pennycook, T. Thundai, and R. J. Warmack, Appl. Phys. Lett. **66**, 34 (1995).
[6] S. Sato, I. Mizushima, K. Miyano, T. Sato, S. Nakamura, Y. Tsunashima, T. Arikado, and N. Uchitomi, Jpn. J. Appl. Phys. **44**, 1169 (2005).
[7] M. Czubanowski, C. Tegenkamp, W. Ernst, and H. Pfnür, Appl. Phys. Lett. **84**, 350 (2004).
[8] P. Cantu, F. Wu, S. Keller, A. E. Romanov, S. P. DenBaars, and J. S. Speck, J. Appl. Phys. **97**, 103534 (2005).
[9] H. K. Cho, J. Y. Lee, and G. M. Yang, Appl. Phys. Lett. **80**, 1370 (2002).
[10] H. Chen, R. M. Feenstra, J. E. Northrup, T. Zywietz, J. Neugebauer, and D. W. Greve, J. Vac. Sci. Technol. B **18**, 2284 (2000).
[11] N. Sharma, P. Thomas, D. Tricker, and C. Humphreys, Appl. Phys. Lett. **77**, 1274 (2000).
[12] H. Shi and D. Lederman, J. Appl. Phys. **87**, 6095 (2000).
[13] A. Nakano, M. E. Bachlechner, R. K. Kalia, E. Lidorikis, P. Vashishta, G. Voyiadjis, T. J. Campbell, S. Ogata, and F. Shimojo, Comput. Sci. Eng. **3**, 56 (2001).
[14] D. Wolf, V. Yamakov, S. R. Phillpot, A. Mukherjee, and H. Gleiter, Acta Mater. **53**, 1 (2005).
[15] M. Marder, Int. J. Refract. Hard Met. **130**, 517 (2004).
[16] S. C. Jain, A. H. Harker, A. Atkinson, and K. Pinardi, J. Appl. Phys. **78**, 1630 (1995).
[17] L. Nicola, E. van der Giessen, and A. Needleman, J. Appl. Phys. **93**, 5920 (2003).
[18] R. Panat and K. J. Hsia, Proceedings of the Royal Society of London, Series A, Mathematical, Physical and Engineering Sciences, 460, 1957–1979 (2004).
[19] C. Wei, K. Cho, and D. Srivastava, Phys. Rev. B **67**, 115407 (2003).
[20] F. F. Abraham and H. Gao, Phys. Rev. Lett. **84**, 3113 (2000).
[21] R. D. Deegan, S. Chheda, L. Patel, M. Marder, H. L. Swinney, J. Kim, and A. de Lozanne, Phys. Rev. E **67**, 066209 (2003).
[22] V. Yamakov, D. Wolf, S. R. Phillpot, A. K. Mukherjee, and H. Gleiter, Nat. Mater. **3**, 43 (2004).
[23] I. Szlufarska, R. K. Kalia, A. Nakano, and P. Vashishta, Phys. Rev. B **71**, 174113 (2005).
[24] M. Li and R. L. B. Selinger, Phys. Rev. B **67**, 134108 (2003).
[25] E. T. Seppälä, J. Belak, and R. E. Rudd, Phys. Rev. B **69**, 134101 (2004).
[26] N. Bernstein and D. W. Hess, Phys. Rev. Lett. **91**, 025501 (2003).
[27] J. R. Chelikowsky, Phys. Rev. Lett. **60**, 2669 (1988).
[28] J. F. Justo, M. Z. Bazant, E. Kaxiras, V. V. Bulatov, and S. Yip, Phys. Rev. B **58**, 2539 (1998).
[29] E. van Veenendaal, H. M. Cuppen, W. J. P. van Enckevort, J. van Suchtelen, A. J. Nijdam, M. Elwenspoek, and E. Vlieg, J. Micromech. Microeng. **11**, 409 (2001).
[30] V. R. Coluci and M. A. Cotta, Phys. Rev. B **61**, 13 703 (2000).
[31] M. T. Lung, C.-H. Lam, and L. M. Sander, Phys. Rev. Lett. **95**, 086102 (2005).
[32] M. E. Bachlechner, R. K. Kalia, A. Nakano, A. Omeltchenko, P. Vashishta, I. Ebbsjö, A. Madhukar, and G. L. Zhao, J. Eur. Ceram. Soc. **19**, 2265 (1999).
[33] J. W. Kim and H. W. Yeom, Phys. Rev. B **67**, 035304 (2003).
[34] G. L. Zhao and M. E. Bachlechner, Europhys. Lett. **37**, 287 (1997).
[35] G. L. Zhao and M. E. Bachlechner, Phys. Rev. B **58**, 1887 (1998).
[36] H. Balamane, T. Halicioglu, and W. A. Tiller, Phys. Rev. B **46**, 2250 (1992).
[37] F. H. Stillinger and T. A. Weber, Phys. Rev. B **31**, 5262 (1985).
[38] J. Tersoff, Phys. Rev. B **37**, 6991 (1988).
[39] J. Tersoff, Phys. Rev. B **38**, 9902 (1988).
[40] S. J. Cook and P. Clancy, Phys. Rev. B **47**, 7686 (1993).
[41] Y. M. Juan, Y. Sun and E. Kaxiras, Philos. Mag. Lett. **73**, 233 (1996).
[42] M. Z. Bazant, E. Kaxiras, and J. F. Justo, Phys. Rev. B **56**, 8542 (1997).
[43] D. Choudhary and P. Clancy, J. Chem. Phys. **122**, 154509 (2005).
[44] M. J. Demkowicz and A. S. Argon, Phys. Rev. B **72**, 245205 (2005).
[45] M. J. Demkowicz and A. S. Argon, Phys. Rev. B **72**, 245206 (2005).
[46] M. Posselt, F. Gao and D. Zwicker, Phys. Rev. B **71**, 245202 (2005).
[47] L. Nurminen, F. Tavazza, D. P. Landau, A. Kuronen, and K. Kaski, Phys. Rev. B **67**, 035405 (2003).
[48] D. Holland and M. Marder, Phys. Rev. Lett. **80**, 746 (1998).
[49] D. Holland and M. Marder, Phys. Rev. Lett. **81**, 4029 (1998).
[50] J. A. Hauch, D. Holland, M. P. Marder, and H. L. Swinney, Phys. Rev. Lett. **82**, 3823 (1999).
[51] D. Srivastava, T. Halicioglu, and T. A. Schoolcraft, J. Vac. Sci. Technol. A **17**, 657 (1999).
[52] L. E. Carter and E. A. Carter, Surf. Sci. **323**, 39 (1995).
[53] L. E. Carter and E. A. Carter, J. Vac. Sci. Technol. A **12**, 2235 (1994).
[54] L. E. Carter, S. Khobabandeh, P. C. Weakliem, and E. A. Carter, J. Chem. Phys. **100**, 2277 (1994).
[55] F. H. Stillinger and T. A. Weber, Phys. Rev. Lett. **62**, 2144 (1989).
[56] D. Kohen, J. C. Tully, and F. H. Stillinger, Surf. Sci. **397**, 225 (1998).
[57] P. Vashishta, R. K. Kalia, A. Nakano, W. Li, and I. Ebbsjö, *Molecular Dynamics Methods and Large-scale Simulations of Amorphous Materials*" in *Amorphous Insulators and Semiconductors*, edited by M. F. Thorpe and M. I. Mitkova (NATO ASI, 1996), p. 151.
[58] C. K. Loong, P. Vashishta, R. K. Kalia, and I. Ebbsjö, Europhys. Lett. **31**, 201 (1995).
[59] A. Nakano, R. K. Kalia, and P. Vashishta, Phys. Rev. Lett. **75**, 3138 (1995).

[60] K. Tsuruta, A. Nakano, R. K. Kalia, and P. Vashishta, J. Am. Ceram. Soc. **81**, 433 (1998).
[61] F. Abraham, Adv. Phys. **35**, 1 (1986).
[62] M. Tuckerman, B. J. Berne, and G. J. Martyna, J. Chem. Phys. **97**, 1990 (1992).
[63] D. Cao, "Pair Distribution Functions in Molecular Dynamics Simulations of Interfaces." Ph.D. thesis, West Virginia University, 2006.